Received: 6 May 2020 | Revised: 10 June 2020 | Accepted: 19 June 2020

DOI: 10.1002/aoc.5930

Applied Organometallic Chemistry WILEY

FULL PAPER

Cobalt(II)/(III) complexes bearing a tetradentate thiosemicarbazone: Synthesis, experimental and theoretical characterization, and electrochemical and antioxidant properties

Büşra Kaya[1] | **Duygu Akyüz**[2] | **Tuncay Karakurt**[3] | **Onur Şahin**[4] | **Atıf Koca**[5] | **Bahri Ülküseven**[1]

[1]Department of Chemistry, Engineering Faculty, Istanbul University-Cerrahpasa, 34320, Avcilar, Istanbul, Turkey

[2]Department of Chemistry, Gebze Technical University, 41400, Gebze, Kocaeli, Turkey

[3]Department of Chemical and Process Engineering, Faculty of Engineering-Architecture, Kırsehir Ahi Evran University, 40100, Kırsehir, Turkey

[4]Department of Occupat Health & Safety, Faculty of Health Sciences, Sinop University, Sinop, TR-57000, Turkey

[5]Chemical Engineering Department, Engineering Faculty, Marmara University, Göztepe, Istanbul, 34722, Turkey

Correspondence
Bahri Ülküseven. Department of Chemistry, Engineering Faculty, Istanbul University-Cerrahpasa, 34320, Avcilar. Istanbul, Turkey.
Email: bahseven@istanbul.edu.tr

Funding information
Scientific and Technological Research Application and Research Center, Sinop University, Turkey; Turkish Academy of Sciences (TUBA); Scientific Research Projects Coordination Unit of Istanbul University-Cerrahpasa; Turkish Academy of Sciences (TUBA); Scientific Research Projects Coordination Unit of Istanbul University-Cerrahpasa

New cobalt complexes, **Co1** and **Co2**, were synthesized starting from acetylacetone-*S*-methylthiosemicarbazone. The square planar cobalt(II) and octahedral cobalt(III) complexes were characterized by FT-IR, UV–visible, ^{1}H NMR, and X-ray diffraction spectroscopies and mass spectrometry. Frontier orbitals of the complexes were theoretically obtained to better understand the complex structures and intermolecular interactions. The electrochemical behaviors of **Co1** and **Co2** were investigated and the results were evaluated by comparing with each other and with similar published compounds to determine their possible usage in various electrochemical technologies, such as energy storage devices, electrocatalysts, and electrosensors. Metal-based oxidation at around 0 V and metal-based reduction at around −1.0 V indicated that these complexes are valuable for the proposed applications. By determining the trolox equivalent antioxidant capacity and the radical scavenging activity of the cobalt complexes, the compatibility between the antioxidant qualification, redox, and theoretical calculation results was discussed.

KEYWORDS
antioxidant potential, cobalt complexes, density functional theory, electrochemistry, thiosemicarbazone

1 | INTRODUCTION

Comprehending basic features of electron transfer reactions in functional materials is not only a demanding scientific mission but also a necessity to investigate the prediction of their practical usage. It thus comes as no surprise that efforts have been made to qualitatively and quantitatively investigate redox processes in complexes of redox active metals such as cobalt.

The molecules of metal complexes have two redox regions consisting of a metal center and a ligand. It has been well documented that the ligand generally exhibits one-electron reduction and oxidation under normal conditions.[1,2] However, the metal center plays an important role in the level of redox activity of these complexes. Expanding the redox activity of organic ligands by redox active metals increases the number of total transformed electrons, which extends the usability of the complexes in energy conversion and storage applications due to their possible high specific capacity. It is known that the redox couples of metal complexes are considerably affected by the nature of substituents on the ligand,[3–8] so detailed redox characterizations of many metal complexes have been examined to find material for possible applications.

Various metal complexes of salen-type ligands have shown multiple voltammetric waves arising from electron transfer in the metal center and/or the ligand. There are many reports on cobalt complexes with a salen ligand, but studies on those with N_2O_2-thiosemicarbazone are few.[9,10] Moreover, experimental studies on cobalt–salen complexes demonstrating cobalt-based electron transfer reactions are very limited.[7,8]

Although thiosemicarbazones and metal complexes are known for their various biological activities, some have also been investigated for their biosensor and optical material properties.[11–15] For the detection of the copper ions, a thiosemicarbazone of a propanedione derivative has been recommended as a chromogenic optical sensor.[16] A thermally resistant zinc(II) complex of 4-methoxybenzaldehyde-thiosemicarbazone has been investigated as a potential nonlinear optical material.[12] The copper(II)[17,18] and cadmium(II)[19] complexes of some thiosemicarbazones have been reported as suitable compounds to produce some optical materials.

In 1987 and 1989, cobalt(II) complexes of N_2O_2-chelating *S*-alkylthiosemicarbazones were obtained using salicylaldehyde derivatives.[9,10] However, cobalt complexes of the thiosemicarbazones with a salen-like but asymmetric N_2O_2 donor set have not been studied for the above-mentioned applications. Here, we synthesized four- and six-coordinated cobalt complexes bearing tetradentate thiosemicarbazone ligands to determine their basic properties for bio- and optic-sensor applications and also demonstrated the relationship between antioxidant capacity and redox properties (Figure 1). The novel complexes **Co1** and **Co2** were structurally characterized using analytical and spectroscopic methods. Redox properties were determined with cyclic voltammetry (CV), square wave voltammetry (SWV), and *in situ* spectroelectrochemical (SEC) measurements. The antioxidant capacities of the complexes were determined by 1,1-diphenyl-2-picryl hydrazyl (DPPH) free radical scavenging assay and Cupric Reducing Antioxidant Capacity (CUPRAC) methods, and the correlation between the redox data and antioxidant capacity is discussed. In addition, detailed computations were performed using the sets DFT/B3LYP and LanL2DZ to confirm the experimental findings and to determine the basic data for the structural features.

2 | EXPERIMENTAL

2.1 | Materials and physical measurements

All chemicals were pure or analytical reagent grade. Elemental analyses were obtained on a Thermo Finnigan Flash EA 1112. Magnetic moments were measured by the Gouy technique (on a Sherwood Sci. MK I model) at room temperature. FT-IR data were obtained by an Agilent Cary 630 spectrophotometer with an Attenuated Total Reflectance (ATR) unit in the 4000–600 cm^{-1} range and ^1H NMR spectra by a Varian UNITY INOVA 500 MHz spectrometer. UV–visible (UV–Vis) spectra were recorded on an Ocean Optics QE65000 diode array spectrophotometer. Electrospray ionization mass spectra (ESI-MS) were obtained on a Thermo Finnigan LCQ Advantage MAX spectrometer.

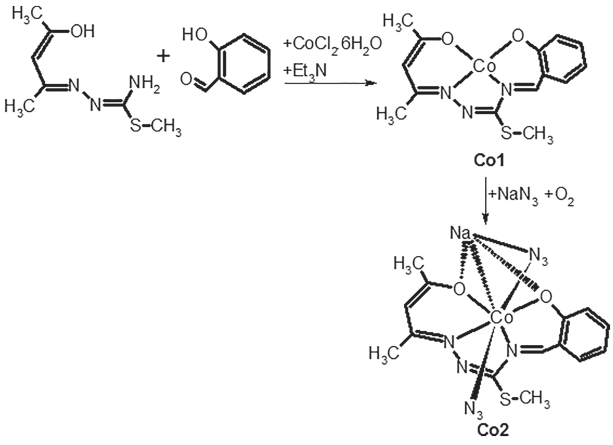

FIGURE 1 Synthesis scheme of cobalt complexes

For X-ray diffraction analysis, suitable crystals of complexes **Co1** and **Co2** were selected for data collection, which was performed on a Bruker D8-QUEST diffractometer using graphite-monochromatic Mo-K_α radiation at 296 K (Table 2). The H atoms were located from different maps and treated as riding atoms with C–H distances of 0.93–0.96 Å. The procedures used for our analysis were solved by direct methods[20] then refined by full-matrix least-squares methods and SHELXL-2013.[21] Data collection was by Bruker APEX2,[22] molecular graphics by MERCURY,[23] and the solution by WinGX.[24]

2.2 | Synthesis

The starting material, acetylacetone-*S*-methylthiosemi -carbazone hydrogen iodide, was prepared by reaction of acetylacetone and *S*-methylthiosemicarbazide hydrogen iodide according to literature methods.[25–27] Characterization data for the cream-colored compound are: yield 2.42 g, 70%; m.p. 160°C. Anal. calcd for $C_7H_{14}N_3OSI$ (315.17): C 26.68, H 4.48, N 13.33, S 10.17; found: C 26.51, H 4.23, N 13.07, S 9.91%. FT-IR: $\nu_{as}(NH_2)$ 3,327, $\nu_s(NH_2)$ 3,260, ν(OH) 3,184, $\delta(NH_2)$, $\nu(C{=}N^1)$, $\nu(N^2{=}C)$ 1,637–1,539. UV–Vis (in 10^{-5} M $CHCl_3$, λ_{max} [nm], logε [dm^3 cm^{-1} mol^{-1}]): 242 (5.04), 252 (5.03), 361 (3.80). ^{1}H NMR: 9.39, 8.95 (*cis*/*trans* ratio: 1/3, s, 2H, N*H*$_2$), 7.70 (s, 1H, O*H*), 3.23 (s, 2H, –C*H*$_2$–), 2.59 (s, 3H, S–C*H*$_3$), 2.08 (s, 3H, C–C*H*$_3$), 1.73 (s, 3H, C–C*H*$_3$).

2.2.1 | N^1-acetylacetone-N^4–2-hydroxybenzylidene-*S*-methylthiosemicarbazidato-cobalt(II) (Co1)

0.24 g (1 mmol) of $CoCl_2.6H_2O$ was added with stirring to a methanolic solution (10 ml) of 0.32 g (1 mmol) of acetylacetone-*S*-methylisothiosemicarbazone hydrogen iodide and 0.1 ml (1 mmol) of 2-hydroxybenzaldehyde. After refluxing the mixture for 15 min, 0.2 ml of Et_3N was added and then refluxing was continued for a further 2 hr. The precipitate, a brown-colored solid product, was crystallized from a mixture of ethanol-dichloromethane (1:1). Yield 0.14 g, 40%; m.p. 223°C; μ_{eff} (BM): 3.34. Anal. calcd for $C_{14}H_{15}N_3O_2SCo$ (348.28): C 48.28, H 4.34, N 12.06, S 9.21; found: C 48.57, H 4.23, N 11.77, S 9.63%. FT-IR: see Table 4. UV–Vis (in 10^{-5} M $CHCl_3$, λ_{max} [nm], logε [dm^3 cm^{-1} mol^{-1}]): 241 (5.05), 297 (4.90), 396 (4.67), 495 (4.63), 548 (4.32). *m*/*z* (+c ESI-MS, % relative abundance): 348.1 [M] (100.00), 695.7 [2M–1H] (70.48), 349.1 [M + 1H] (49.12), 696.7 [2M] 47.64.

2.2.2 | Sodium diazido-N^1-acetylacetone-N^4–2-hydroxybenzylidene-*S*-methylthiosemicarbazidato-cobalt(III) (Co2)

A solution of 0.2 g (0.57 mmol) of **Co1** in 10 ml of methanol-dichloromethane (1:1) was slowly air bubbled and then 0.1 g (1.5 mmol) of NaN_3 dissolved in 10 ml of methanol was added. The mixture was refluxed by continuing aerial oxidation for 4 hr and the product was filtered off. The clear solution was allowed to stand at room temperature. After 24 hr, dark-brown crystals of the complex formed a solid phase. Yield 0.09 g, 35%; m. p. > 350°C; μ_{eff} (BM): approx. 0. Anal. calcd for $C_{14}H_{15}N_9O_2SCoNa$ (455.33): C 36.93, H 3.32, N 27.69, S 7.04; found: C 36.47, H 3.51, N 27.28, S 6.77%. FT-IR: see Table 4. UV–Vis (in 10^{-5} M $CHCl_3$, λ_{max} [nm], logε [dm^3 cm^{-1} mol^{-1}]): 242 (4.99), 357 (4.75), 509 (4.43). *m*/*z* (+c ESI-MS, % relative abundance): 802.5 [2M–(2N_3 + Na + H)] (100.00), 412.7 [M–N_3] (66.22), 760.6 [2M–(3N_3 + Na + H)] (41.12), 803.5 [2M–(2N_3 + Na)] 31.71. ^{1}H NMR: 7.85 (s, 1H, $N^4{=}CH$), 7.55 (d, 1H, *d*), 7.26 (t, 1H, *c*), 7.19 (d, 1H, *a*), 6.50 (t, 1H, *b*), 5.03 (s, 1H, =C*H*), 2.75 (s, 3H, S–C*H*$_3$), 2.52 (s, 3H, C–C*H*$_3$), 2.22 (s, 3H, C–C*H*$_3$).

2.3 | Electrochemical measurements

CV and SWV measurements were performed on a potentiostat (GAMRY Instruments, Reference 600 Potentiostat/Galvanostat/ZRA) coupled by following the procedure in the literature.[28] The CV and SWV measurements used a three-electrode system with a glassy carbon electrode (GCE) as the working electrode with a surface area of 0.072 cm^2, a Pt wire counter, and a Ag/AgCl reference electrode. The *in situ* UV–Vis spectroelectrochemical and electrocolorimetric measurements used an Ocean Optics QE65000 diode array spectrophotometer coupled with a potentiostat. The data were obtained in a thin-layer quartz spectroelectrochemical cell with a three-electrode configuration using a Pt tulle working electrode following the literature procedure.[28]

2.4 | Theoretical calculations

Molecular modeling of complexes was carried out using the Gaussian 09 program[29] and basic functional density theory DFT/B3LYP[30,31] with the 6–31G (d, p)[32] base set for the C, N, O, H atoms and the LanL2DZ[33–35] base set for cobalt(II) and cobalt(III) atoms.

2.5 | Antioxidant capacity and activity tests

Total antioxidant capacity of the complexes (**Co1** and **Co2**) was assessed according to the CUPRAC method.[36] By using the measurements at 450 nm, Trolox equivalent antioxidant capacity coefficients (TEAC) coefficients were calculated as the molar absorptivity ratio of each compound to that of the trolox method (ε_{trolox}: 1.67×10^4 L mol^{-1} cm^{-1}).

DPPH free radical scavenging assay was performed using the following procedure. DPPH radical solution in methanol (100 μM) was reacted with 5, 10, 15, 20, and 25 μM of the compounds for 30 min. The decrease in absorbance was recorded at 515 nm.[37] The IC_{50} values giving minimum concentration required to scavenge 50% of DPPH radicals were calculated. The assays were carried out in triplicate at room temperature and the results expressed as mean value ± standard deviation.

3 | RESULTS AND DISCUSSION

3.1 | Synthesis, spectral, and structural studies

Condensation of *S*-methylthiosemicarbazone and 2-hydroxybenzaldehyde by the template effect of cobalt(II) yielded the square planar complex **Co1**, with five- and six-membered chelate rings. Formation of dibasic N_2O_2-thiosemicarbazidato ligand by template condensation and its coordination to cobalt(II) are simultaneous. Completion of the reaction was monitored by FT-IR spectra. Because OH and NH_2 groups react in this process (see Figure 1), the bands ν(OH) at 3,184 cm^{-1}, $\nu(NH_2)$ at 3,327, and 3,260 cm^{-1} for the starting material were not observed in the FT-IR spectrum of complex **Co1**. In addition, a new band appeared at 1,558 cm^{-1} for the $\nu(N^4{=}C)$ vibration arising from condensation of NH_2 of *S*-methylthiosemicarbazone and CH=O of salicylaldehyde.

The value of 3.34 BM obtained at room temperature for **Co1** indicates the high-spin structure of the cobalt(II) center. The μ_{eff} value is lower than the expected values (4.4–4.8 BM) for tetrahedral cobalt(II) complexes[38] and indicates that the locations of donor atoms (O, N, N, O) of the thiosemicarbazone are in a mold close to square planar geometry. ESI-MS measurement for **Co1** gave a peak at 348.1 (100% relative abundance) corresponding to the mole weight of the complex molecule (Supporting Information Figure S5).

An anionic structure with azide ions in axial positions was intended by considering the octahedral geometry tendency of cobalt(III) ions. Using complex **Co1** as the starting material, a series of reactions was carried out involving aerial oxidation of the cobalt(II) center and addition of NaN_3. Repeated reactions resulted in the formation of a neutral complex containing a sodium atom instead of the anionic structure (see Figures 1 and 2b). Complex **Co2** has asymmetrical N_2O_2-chelating thiosemicarbazone and azide ligands and its polymer construction is similar to that of cobalt(III) complexes of symmetrical salen ligands.[39–41]

The FT-IR spectrum of **Co2** does not include the OH and NH_2 bands of the *S*-methylthiosemicarbazone that are seen for complex **Co1**. The spectrum contains bands at 2040 and 2014 cm^{-1} arising from stretching vibrations of the azide as co-ligand in addition to the bands similar to those for **Co1**. The octahedral complex **Co2** is diamagnetic and the cobalt(III) center is in a low-spin state because of the strong field of the azide ligands.[39] The ^{1}H NMR spectrum in DMSO-d_6(dimethyl sulfoxide-d_6) of complex **Co2** does not contain any signal related to the OH and NH_2 protons of the starting material. This finding supports the FT-IR data since it shows that these groups react by giving their protons. The proton signals belonging to the acetylacetone, phenyl, and imine groups

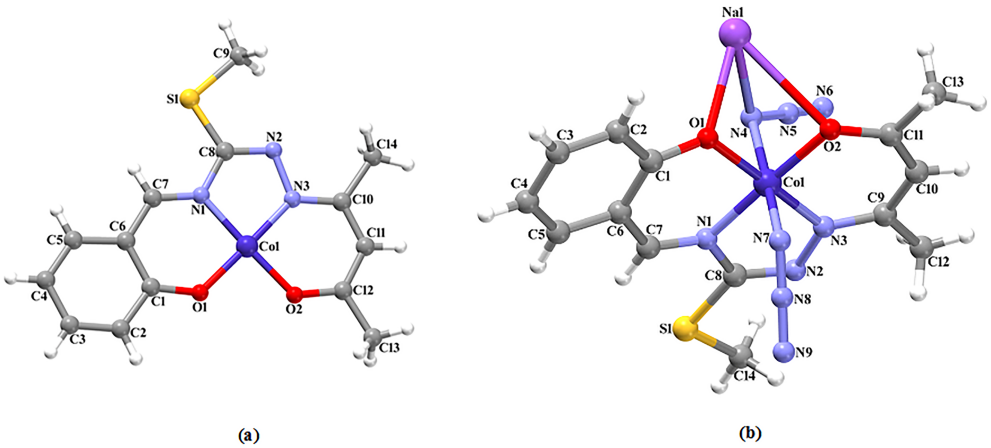

FIGURE 2 The molecular structures of **Co1** (a) and **Co2** (b) showing the atom numbering schemes

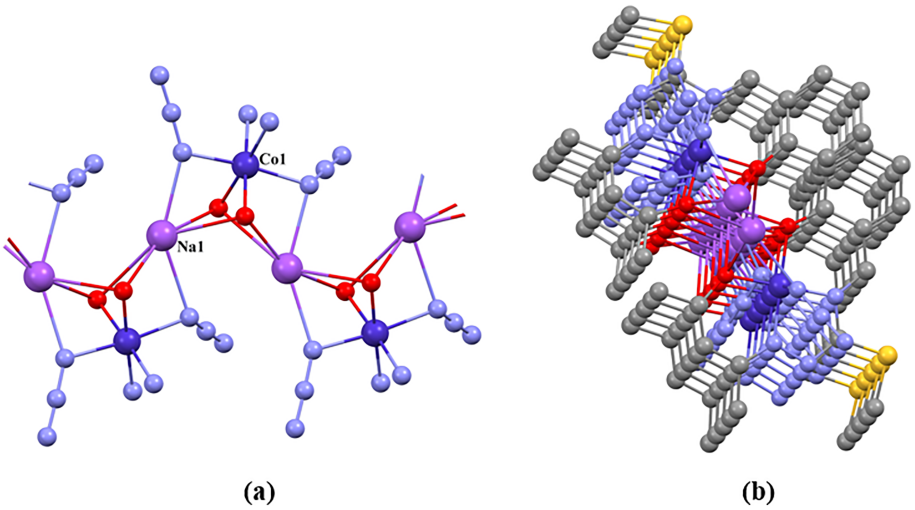

FIGURE 3 The 1D (a) and 3D (b) supramolecular network in **Co2**

demonstrate that the square planar base in **Co1** is protected in complex **Co2** (Supporting Information Figure S7). The mass spectrum of **Co2** has peaks indicating some fragments associated with two cobalt-centered structure instead of a mononuclear unit (Figure 2b). The peaks for 2M–($2N_3$ + Na + H), 2M–($2N_3$ + Na), and 2M–($3N_3$ + Na + H) correspond to the dimeric parts of this polymer. As well as these, a fragment M–N_3 (66.22% relative abundance), originating from the single unit, was observed (Supporting Information Figure S6).

3.2 | X-ray crystallography

The molecular structures of **Co1** and **Co2**, with their atom numbering schemes, are shown in Figure 2. The asymmetric unit of complex **Co1** contains one cobalt(II) ion and one dibasic thiosemicarbazidato ligand, while the asymmetric unit of complex **Co2** contains one cobalt(III) ion, one Na(I) ion, one ligand and two azides as co-ligands. In complex **Co1**, the cobalt(II) is coordinated by two oxygen atoms [Co1–O1 = 1.820 (12) Å and Co1–O2 = 1.835 (13) Å] and two nitrogen atoms [Co1–N1 = 1.860 (14) Å and Co1–N3 = 1.818 (16) Å] (see Supporting Information Table S1) from the ligand, thus showing distorted square planar coordination geometry. In **Co1**, atom C9 in the molecule at (x, y, z) acts as hydrogen-bond donor to the O2 atom in the molecule at ($1 - x$, $2 - y$, $1 - z$), so forming a C(7) chain which runs parallel to the [101] direction (Supporting Information Figure S2).

As seen in the crystal structure of **Co2** (Figure 3a), the unit NaCo(L)(N_3)$_2$ has one dibasic thiosemicarbazone and two azide ions as ligands. Sodium atoms with octahedral environments act as a bridge in this polymer structure. The cobalt atom is coordinated with the two oxygen and two nitrogen atoms of the thiosemicarbazidato and two nitrogen atoms from two azide molecules. The bond lengths (Å) Co1–O = 1.924 (11), Co1–O2 = 1.901 (11), Co1-N1 = 1.880(13), Co1–N3 = 1.879 (13), [Co1–N4 = 1.999 (11) and Co1–N7 = 1.950 (11) display distorted octahedral coordination geometry (see Supporting Information Table S1). When the Na(I) ion is located on a center of symmetry and coordinated by four oxygen atoms [Na1–O1 = 2.374 (12) Å and Na1–O2 = 2.462 (13) Å] and two nitrogen atoms [Na1–N4 = 2.523 (12) Å] from the neighboring thiosemicarbazone ligands, a distorted trigonal prismatic coordination geometry is obtained. Adjacent [CoL(N_3)$_2$] units are bridged by Na(I) to generate a one-dimensional (1D) coordination polymer (Figure 3a) that runs parallel to the [100] direction, with a Co·····Co distance of 6.136 Å. Adjacent 1D coordination polymers are further joined by C–H·····π interactions (Supporting Information Table S2), generating a 3D supramolecular network (Figure 3b).

Molecules similar to complex **Co2** are salen complexes with a symmetrical N_2O_2 donor set. Azide anions are also in the axial position in the cobalt(III) complexes of salen ligands obtained from 1,3-diaminopropane[40] and 1,2-diaminocyclohexane,[41] and their Co–N (azide) bonds are approximately 1.96 Å. In complex **Co2**, the Co–N (azide) distances are different [1.999 (11) and 1.950 (11) Å] due to the asymmetric N_2O_2 set. The Na–N (azide) bonds of **Co2** are 0.05–0.097 Å longer than those of these salen complexes. Each of the bond lengths in the O–Na–O bridges is different, but the values are compatible with those of the salen complexes.

3.3 | Voltammetric measurements

Electrochemical characterizations of complexes **Co1** and **Co2** were carried out with CV and SWV in DMSO/TBAP (Tetrabutylammonium perchlorate) electrolyte on a GCE.

TABLE 1 Electrochemical data for the complexes in DMSO/TBAP solution

	Redox processes					
	Red_2			Red_1		
	$[Co^{I}L]^{1-}/[Co^{I}L^{1-}]^{2-}$			$[Co^{II}L]/[Co^{I}L]^{1-}$		
Complexes	$E_{1/2}$ (V)	ΔE_p (mV)	$I_{p,a}/I_{p,c}$	$E_{1/2}$ (V)	ΔE_p (mV)	$I_{p,a}/I_{p,c}$
Co1	−2.01	67	0.48	−1.14	77	0.54
Co2	−2.07	124	0.34	−1.17	87	0.56
	Oxd_1			Oxd_2		
	$[Co^{II}L]/[Co^{III}L]^{1+}$			$[Co^{III}L]^{1+}/[Co^{III}L^{1+}]^{2+}$		
	$E_{1/2}$ (V)	ΔE_p (mV)	$I_{p,a}/I_{p,c}$	$E_{1/2}$ (V)	ΔE_p (mV)	$I_{p,a}/I_{p,c}$
Co1	−0.06	65	0.94	1.11	120	0.38
Co2	−0.11 (−0.37)	–	–	0.72 (0.95)	–	–

TABLE 2 Crystal data and structure refinement parameters for the complexes

	Co1	**Co2**
Empirical formula	$C_{14}H_{15}CoN_3O_2S$	$C_{14}H_{15}CoN_9NaO_2S$
Formula weight	348.28	455.33
Crystal system	Orthorhombic	Orthorhombic
Space group	$Pna2_1$	$Pna2_1$
a (Å)	7.4748 (11)	7.228 (3)
b (Å)	21.993 (4)	16.742 (6)
c (Å)	8.8571 (15)	14.949 (4)
V (Å^3)	1456.0 (4)	1809.0 (10)
Z	4	4
Diffractometer	BRUKER D8-QUEST	
Temperature (K)	296	
D_c (g cm^{-3})	1.589	1.672
μ (mm^{-1})	1.33	1.12
θ range (°)	2.9–26.4	3.1–26.5
Measured refls.	7,415	20,968
Independent refls.	2,706	3,518
R_{int}	0.088	0.095
S	1.25	1.08
R1/wR2	0.094/0.225	0.081/0.184
$\Delta\rho_{max}/\Delta\rho_{min}$ (eÅ^{-3})	0.66/−0.60	0.98/−0.69

TABLE 3 The TEAC coefficients and DPPH results as IC_{50}

Compound	**TEAC value**	**DPPH IC_{50} (μM)**
Co1	0.50 ± 0.08	259
Co2	1.66 ± 0.15	111

CVs and SWVs were analyzed to derive basic redox parameters, including half-wave peak potentials ($E_{1/2}$), the ratio of anodic and cathodic peak currents (I_{pa}/I_{pc}), and peak potential separations (ΔE_p) of the redox couples of the complexes (see Table 1). Under the dynamic potentiometric polarization of the working electrode both of the complexes undergo two reductions and two oxidations within the potential window of the DMSO/TBAP electrolyte.

The CV and SWV diagrams of **Co1** are shown in Figure 4. It gives the $[Co^{II}L]/[Co^{III}L]^{1+}$ process at −0.06 V (Oxd1) and the $[Co^{III}L]^{1+}/[Co^{III}L^{+1}]^{2+}$ process at 1.11 V (Oxd2). This figure also illustrates the $[Co^{II}L]/[Co^{I}L]^{1-}$ process at −1.14 V (Red1) and the $[Co^{I}L]^{1-}/[Co^{I}L^{-1}]^{2-}$ process at −2.01 V (Red2) during the negative potential scans. In addition to the main couples of **Co1**, small waves were observed during the reverse potential scans due to the redox processes of some products formed by sequential reactions. Observation of these small waves illustrates the chemical instability of the electrogenerated dianionic species. However, voltammetric measurements with different vertex potentials indicated that **Co1** is chemically and electrochemically reversible when the CV cycles were recorded between 0.50 and −1.50 V.

When **Co1** was polymerized by azide ligands to form **Co2**, the electrochemical responses were not significantly influenced. The peak positions and behaviors of the complex were slightly differentiated after the polymerization. The peaks of **Co2** shift to the negative side with respect to those of **Co1**. Moreover, the peaks of **Co2** derivatives from reversibility with respect to those of **Co1**.

As shown in Figure 5, **Co2** represents electron transfer reactions at −0.11 and 0.95 V for the $[Co^{II}L]/[Co^{III}L]^{1+}$ and $[Co^{III}L]^{1+}/[Co^{III}L^{+1}]^{2+}$ processes and −1.17 and −2.07 V for the $[Co^{II}L]/[Co^{I}L]^{1-}$ and $[Co^{I}L]^{1-}/$

TABLE 4 The experimental and theoretical FT-IR bands (cm^{-1}) for the complexes

	Co1		Co2	
Band	**Exp.**	**Calcd**	**Exp.**	**Calcd**
$\nu(CH)_{phenyl}$	3,025–3,001	3,078–3,041	3,036–2,999	3,085–3,041
$\nu(CH)_{methyl}$	2,940–2,918	2,920–2,850	3,035–3,004	2,923–2,855
$\nu(N{=}N)_{azide}$	–	–	2040, 2014	2056, 2014
$\nu(C{=}N^1)$	1,605	1,557	1,602	1,575
$\nu(N^2{=}C)$	1,570	1,531	1,585	1,554
$\nu(N^4{=}C)$	1,558	1,508	1,576	1,517
$\nu(C{-}N)$	1,118	1,136	1,106	1,127
$\nu(C{-}O)$	1,359	1,371	1,363	1,341

$[Co^{I}L^{-1}]^{2-}$ processes, respectively. All of these redox processes have similar behaviors to those of **Co1**. However, the Red1 process of **Co2** is less reversible. Moreover, the ligand-based oxidation process (Oxd2) splits into two waves due to possible chemical degradation following the first (Oxd1). This finding is evidence for the chemical instability of monocationic species originating in **Co2**.

The redox response and peak assignment data of **Co1** and **Co2** are in harmony with those of Schiff base complexes bearing a symmetric N_2O_2 donor set[3–8] and these assignments are supported by the *in situ* SEC measurements discussed below. For instance, Böttcher and coworkers published electrochemical responses for 15 cobalt(III) derivatives of the N_2O_2 ligands and reported that all complexes illustrated $[Co^{II}L]/[Co^{I}L]^{1-}$ peaks at around −1.00 V and $[Co^{II}L]/[Co^{III}L]^{1+}$ peaks at around 0.20 V.[3] In another study, Chai and coworkers reported$[Co^{II}L]/[Co^{I}L]^{1-}$ peaks at −1.42 V and $[Co^{II}L]/[Co^{III}L]^{1+}$ peaks at around −0.35 V.[4]

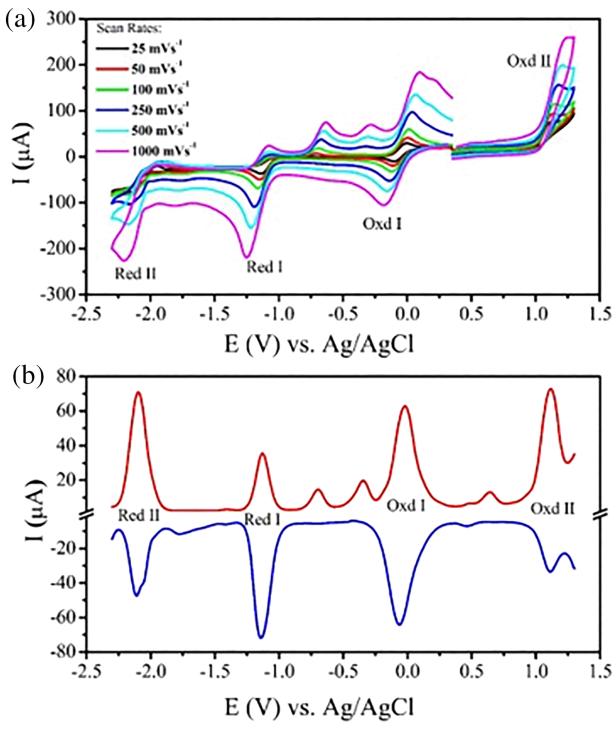

FIGURE 4 CV and SWV of **Co1** in a TBAP/DMSO electrolyte system on a GCE working electrode at different scan rates

The experimental findings demonstrate yet again the important relationship between electrochemical properties and metal type, as seen in nickel(II), manganese(III), iron(III), oxovanadium(IV), and dioxouranium(VI) complexes of N_2O_2-thiosemicarbazones.[42–46]

Multi-electrons and metal-based electron transfer processes for **Co1** and **Co2** at small potentials indicate a functionality for possible electrochemical practices such as energy application of supercapacitors due to the increased Faradic capacitance.

3.4 | Spectroelectrochemical measurements

In situ SEC responses of **Co1** and **Co2** were measured in TBAP/DMSO electrolyte. Both complexes show very similar spectral changes during the electron transfer reactions, so the spectral changes for **Co1** are shown in Figure 6 as an example. Neutral **Co1** gives clear bands at 298, 346, 394, 428, 468, and 562 nm. The bands at lower energy (298 and 346 nm) are attributable to $\pi \rightarrow \pi^*$ transitions associated with the phenyl ring, and the bands at higher energy (394 and 428 nm) arise from $\pi \rightarrow \pi^*$ transitions within the imine chromophore. The bands at 486 and 562 nm correspond to an $n \rightarrow \pi^*$ transition and ligand to metal charge transfer (LMCT), respectively.[3] Under an applied potential of 0.50 V, the LMCT band at 562 nm increased in intensity, while $\pi \rightarrow \pi^*$ transition bands associated with the phenyl ring of the ligand at 394 and 428 nm slightly decreased. Moreover, the band at 468 nm corresponding to the $n \rightarrow \pi^*$ transition[8] did not

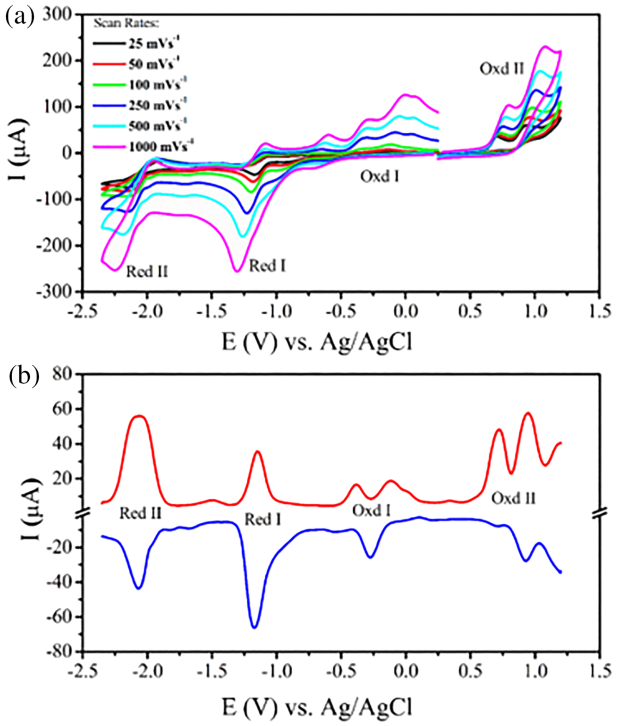

FIGURE 5 CV and SWV of **Co2** in a TBAP/DMSO electrolyte system on a GCE working electrode at different scan rates

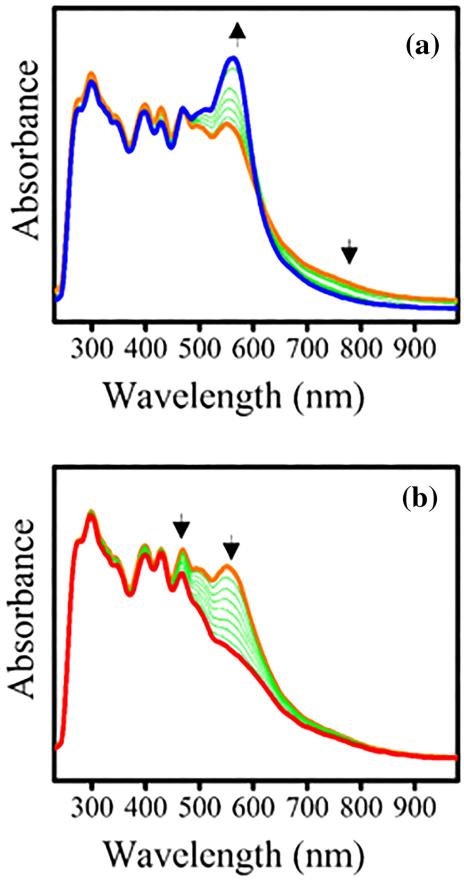

FIGURE 6 *In situ* UV–Vis spectral changes of **Co1** in DMSO/TBAP electrolyte: (a) E_{app} = 0.50 V and (b) E_{app} = −1.20 V

change (Figure 6a). These spectral changes indicate a metal-based oxidation process and support the $[Co^{II}L]/[Co^{III}L]^{1+}$ character of the Oxd1 process.[5–8] During the reduction reaction at −1.20 V (Red1), while the metal to ligand charge transfer (MLCT) band at 562 nm and the band at 468 nm decreased in intensity, the bands at 394 and 428 nm did not change (Figure 6b). These spectral changes show the $[Co^{II}L]/[Co^{I}L]^{1-}$ mechanism of the Red1 process. In the other processes, all bands become low intensity, which indicates the composition and chemical instability of the species generated during the ligand-based redox reactions.

3.5 | Theoretical calculations

3.5.1 | FT–IR

The experimental and calculated band frequencies and the FT-IR spectra of the complexes are shown in Table 4 and Supporting Information Figures S3 and S4, respectively.

The aromatic C–H vibrations were calculated to be in the frequency ranges 3,078–3,041 (for **Co1**) and 3,085–3,041 cm^{-1} (for **Co2**), approximately 40–50 cm^{-1} higher than the experimental values. However, the symmetrical and asymmetrical vibration bands of aliphatic C–H vibrations were found in a lower frequency range than experimental values, probably due to the tendency of the CH_3 protons to bridge in solid state (see Table 4). The stretching modes for the C=N of the complexes were calculated as 1,557, 1,531, and 1,508 cm^{-1} for **Co1** and 1,575, 1,554, and 1,517 cm^{-1} for **Co2**, 27–59 cm^{-1} higher ranges of frequency compared to the experimental bands. The vibration peaks are in the order $C{=}N^1$, N^2 = C, N^4 = C, as in the experimental spectra, and have high density bands similar to those of Schiff bases.[47]

The C–N stretching bands were calculated to be 1136 cm^{-1} for **Co1** and 1127 cm^{-1} for **Co2**, approximately 20 cm^{-1} higher than the experimental values. The calculations gave frequencies of 1,371 and 1,341 cm^{-1}, close to experimental values for the C–O stretching vibrations in **Co1** and **Co2**, respectively. The C=C vibrations were calculated as 1,591 and 1,589 cm^{-1} for **Co1** and **Co2**, respectively, but could not be distinguished in the experimental spectra since they are in the region of the C=N bands. For the sharp N=N bands of the azide ligands in complex **Co2** was found 2056 and 2014 cm^{-1} of the values quite close to those obtained on the ATR device.

The differences observed between experimental and theoretical data may be due to the various intermolecular

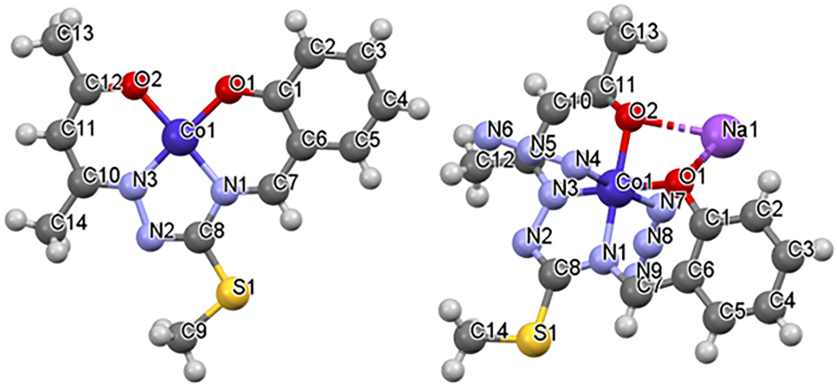

FIGURE 7 Optimized structures of **Co1** and **Co2** complexes

interactions in the solid phase that are not included in the calculations for the single molecule in the gas phase.

3.5.2 | Charge distribution analysis

The optimized structures of the two complex structures are shown in Figure 7. The calculated Mulliken atomic charges of the atoms forming the two complex structures are given in Supporting Information Table S3. It can be seen that the calculated charge on the metal ion is significantly lower than the formal charges, 2+ and 3+, because there is a significant charge transition from O and N atoms to the cobalt center. The central metal ions in both complex structures have mostly 3d, 4s, and 4p orbital arrangement. The arrangement of this ion in the **Co1** complex is [core]$4S^{0.10}$ $3d^{3.31}$ $4p^{0.14}$ and its arrangement in **Co2** is [core]$4S^{0.29}$ $3d^{7.68}$ $4p^{0.57}$ $4d^{0.02}$ $5p^{0.01}$. The occupancies of d orbitals are $3d_{xy}^{0.56104}$ $3d_{xz}^{0.98893}$ $3d_{yz}^{0.9688}$ $3d_{x^2y^2}^{2(0.74435)}$ $d_{z}^{2(0.04646)}$ for **Co1** complex and $3d_{xy}^{1.42825}$ $3d_{xz}^{1.97252}$ $3d_{yz}^{1.95905}$ $3d_{x^2y^2}^{2(0.74435)}$ $3d_{z}^{2(1.36607)}$ $4d_{xy}^{0.00336}$ $4d_{xz}^{0.00228}$ $4d_{yz}^{0.00258}$ $4d_{x^2y^2}^{2(0.00324)}$ $4d_{z}^{2(0.00417)}$ for **Co2** complex. Both oxygen and nitrogen atoms of the ligands contribute to complex formation with 2s and 2p orbitals. In addition, net charges on the active centers of the metal complexes were calculated and it was observed that there was charge transfer from the ligands of both complexes to the central metal ions. When Supporting Information Table S3 is analyzed, L → M charge transfers for the **Co1** and **Co2** complexes can be calculated as 1.725 and 1.399 for the gas phase and 1.621 and 1.458 for the chloroform, respectively. It was observed that charge transfer decreased in **Co1** in chloroform and increased in **Co2**.

3.5.3 | Electronic properties

The frontier orbitals (HOMO: Highest Occupied Molecular Orbital and LUMO: Lowest Unoccupied Molecular Orbital) are also known as electron donor and acceptor groups. They can be used to determine intermolecular charge transfers, and many molecular properties such as ionization potential, electron affinity, chemical reactivity, kinetic stability, electronegativity, and electrophilicity index can be calculated by considering the energy levels.[48,49] The distributions and energy levels of the frontier molecular orbitals (α and β) of the complexes **Co1** and **Co2** are shown in Figure S1. The calculated energy between the αHOMO and the αLUMO is 3.12 eV and between the βHOMO and the βLUMO is 3.08 eV for **Co1** while the calculated energy gap between the HOMO and LUMO of the **Co2** complex is 2.96 eV.

Experimental and calculated UV–Vis spectra of the cobalt complex are given in Figure 8. Free Schiff bases

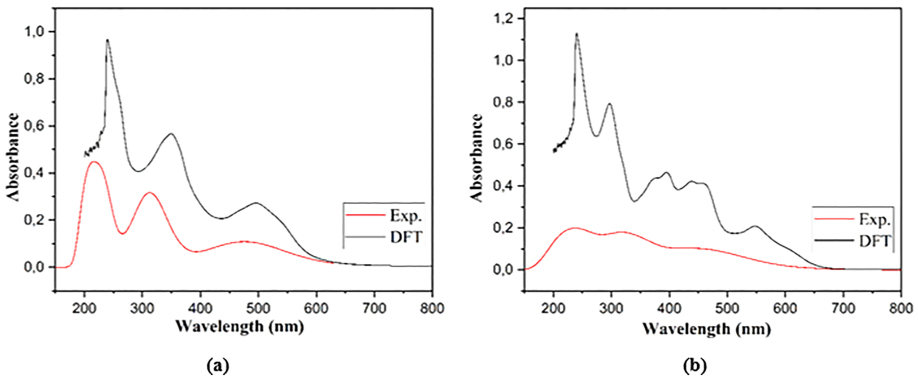

FIGURE 8 Experimental and calculated UV–Vis spectra belonging to (a) **Co1** and (b) **Co2** complexes in the chloroform phase

and their complexes exhibit the bands attributed to the π–π* transitions belonging to the imine C=N and aromatic C=C in the region of 200–300 nm.[47] In accordance with literature data, three major peaks were observed in both experimental and calculated spectra. The first major absorption peaks recorded at 241 nm for **Co1** and 242 nm for **Co2** resulted from the π → π* transitions of the double bonds in the benzene, carbonyl, and imine groups of the complex structures, which were calculated at 221 and 213 nm. The second major peak observed at 297 and 357 nm for the two complex structures originates from the n → π* transitions of the lone pair orbital electrons on the N atom in the imine group, which were calculated at 323 and 309 nm. These n → π* transitions showed hypochromic shifts in the electronic absorption spectra of the complexes. These low-energy region shifts indicate that the ligand is in coordination with the metal ion.[50] In general, wavelengths of compounds containing cobalt for n → π* transitions increased compared to ligands, whereas peaks for the π–π* transition shifted to smaller wavelengths. A third set of major peaks were observed in the complexes at 495 nm for **Co1** and 509 nm for **Co2**. These two peaks were calculated at 435 nm for **Co1** and 476 nm for **Co2**. The major contributions for these transitions are showed in Supporting Information Tables S4 and S5. As seen from these tables, the contributions of the Co(II)/Co(III) atoms play an important role in the αHOMO-2(56%), αHOMO-11(52%), αLUMO+1(62%), βHOMO-3(52%), βHOMO-5(46%), and βLUMO+1(118%) molecular orbitals in the **Co1** complex and the LUMO+1(52%), LUMO+2(61%), HOMO-9(34%), HOMO-10(48%), HOMO-13(53%) molecular orbitals in the **Co2** complex. This means these orbitals are more intense than those of other atoms of the ligand moiety and may be assigned mainly to LMCT, MLCT or d–d transitions.[51] The other orbitals, where ligand atoms are more intense, may be assigned mainly to ligand to ligand charge transfer.

3.6 | Antioxidant assay

TEAC and free radical scavenging activities (IC_{50}) for **Co1** and **Co2** are given in Table 3.

When the TEAC values of the cobalt complexes ae compared with the value for vitamin C (1.02 ± 0.01), the order **Co2** > vitamin C > **Co1** was obtained and complex **Co2** was seen to have an antioxidant capacity comparable to vitamin C. According to the DPPH test results, the complexes **Co1** (IC_{50} 259 μM) and **Co2** (IC_{50} 111 μM) exhibited scavenging activities lower than that of vitamin C (IC_{50} 9 μM). This may be due to the nature of the metal ion,[52] the redox potential,[53] the absence of phenolic OH groups,[54] and the steric hindrance between the complexes and the DPPH radical.[55]

The polymeric cobalt(III) complex (**Co2**) with azide groups performed better than the monomeric cobalt(II) complex (**Co1**) in terms of both antioxidant capacity and radical scavenging activity. The results indicate that electron-rich nitrogen atoms on azide groups in the structure of **Co2** may have a positive effect on the total antioxidant capacity.[42,56] Since the potent antioxidant (essentially reducing) compound will have less positive oxidation and higher reducing potential,[42,57,58] the TEAC and IC_{50} values are compatible with the voltametric ones.

4 | CONCLUSION

The cobalt(II) and cobalt(III) complexes with *S*-methylthiosemicarbazone with an asymmetrical N_2O_2 donor set were examined by experimental and theoretical methods. The square planar complex **Co1** is the first structure obtained starting from acetylacetone. In the novel complex **Co2**, cobalt(III) has an octahedral environment with two azide ions as co-ligands in axial positions. The **Co2** crystal has a 1D coordination polymer bridged with Na(I) as well as a 3D supramolecular structure created by C–H···π interactions.

Electrochemical and SEC measurements showed that both complexes had metal-based oxidation and reduction processes in addition to ligand-based redox. The metal-based redox processes were electrochemically and chemically reversible, but the ligand-based redox processes caused the formation of some chemical species, probably arising from degradation of the organic moiety. These multi-electron metal-based redox activities showed that the complexes could be suitable materials for some practical applications of electrochemistry. Moreover, the compatibility of the redox values of the complexes with the antioxidant test results revealed that electrochemical methods could be developed to use in determining the antioxidant capacities of this class of compounds.

The theoretical calculations also supported the redox properties of the cobalt complexes in addition to the structural analysis data. The energy levels of the frontier orbitals are compatible with the redox potentials and the antioxidant test results. The fact that the HOMO energy of **Co2** (111 eV) is higher than that of **Co1** (85 eV) is the reason why **Co2** is a better reducing agent. So, the negative charge density from the azide ions was verified by the FMO calculations. The results suggest that elaborate theoretical calculations can be used to determine antioxidant capacities like in the spectroscopic and electrochemical methods.

ACKNOWLEDGMENTS

This work was supported by the Scientific Research Projects Coordination Unit of Istanbul University-Cerrahpasa. Atıf KOCA thank the Turkish Academy of Sciences (TUBA) for financial support. The authors acknowledge the Scientific and Technological Research Application and Research Center, Sinop University, Turkey, for the use of the Bruker D8-QUEST diffractometer.

ORCID

Bahri Ülküseven https://orcid.org/0000-0001-6342-1505

REFERENCES

[1] A. H. Kianfar, S. Zargari, *J. Coord. Chem.* **2008**, *61*, 341.
[2] S. Issaadi, D. Haffar, T. Douadi, S. Chafaa, D. Séraphin, M. A. Khan, G. Bouet, *Synth. React. Inorganic, Met. Nano-Metal Chem.* **2005**, *35*, 875.
[3] A. Böttcher, T. Takeuchi, K. I. Hardcastle, T. J. Meade, H. B. Gray, D. Cwikel, M. Kapon, Z. Dori, *Inorg. Chem.* **1997**, *36*, 2498.
[4] L. Q. Chai, J. J. Huang, J. Y. Zhang, Y. X. Li, *J. Coord. Chem.* **2015**, *68*, 1224.
[5] S. Duman, I. Kizilcikli, A. Koca, M. Akkurt, B. Ülküseven, *Polyhedron* **2010**, *29*, 2924.
[6] A. Kilic, E. Tas, B. Deveci, I. Yilmaz, *Polyhedron* **2007**, *26*, 4009.
[7] M. V. Novozhilova, E. A. Smirnova, J. A. Polozhentseva, J. A. Danilova, I. A. Chepurnaya, M. P. Karushev, V. V. Malev, A. M. Timonov, *Electrochim. Acta* **2018**, *282*, 105.
[8] M. Salehi, M. Amirnasr, S. Meghdadi, K. Mereiter, H. R. Bijanzadeh, A. Khaleghian, *Polyhedron* **2014**, *81*, 90.
[9] N. V. Gerbeleu, M. D. Revenko, V. G. Rusu, A. T. Shames, *Theor. Exp. Chem.* **1987**, *23*, 216.
[10] K. M. Indrichan, S. P. Palii, D. V. Zagorevskii, N. V. Gerbeleu, Y. S. Nekrasov, V. B. Arion, *Bull. Acad. Sci. USSR, Div. Chem. Sci.* **1989**, *38*, 2066.
[11] D. Chun-Ying, L. Ze-Hua, S. Yong-Cheng, Y. Xiao-Zeng, *J. Coord. Chem.* **1999**, *47*, 433.
[12] Y. P. Tian, W. T. Yu, C. Y. Zhao, M. H. Jiang, Z. G. Cai, H. Kun Fun, *Polyhedron* **2002**, *21*, 1217.
[13] H. A. Zamani, *Anal. Lett.* **2008**, *41*, 1850.
[14] M. Bakir, O. Brown, *J. Mol. Struct.* **2009**, *930*, 65.
[15] N. Moorthy, P. C. Jobe Prabakar, S. Ramalingam, S. Periandy, G. V. Pandian, *J Theor Comput Sci* **2015**, *2*, 2.
[16] M. A. Chamjangali, S. Soltanpanah, N. Goudarzi, *Sens. Actuators B* **2009**, *138*, 251.
[17] R. C. Chikate, A. R. Belapure, S. B. Padhye, D. X. West, *Polyhedron* **2005**, *24*, 889.
[18] W. S. Wu, W. D. Cheng, D. S. Wu, H. Zhang, Y. J. Gong, Y. Lu, *Inorg. Chem. Commun.* **2006**, *9*, 559.
[19] Y. P. Tian, C. Y. Duan, C. Y. Zhao, X. Z. You, T. C. W. Mak, Z. Y. Zhang, *Inorg. Chem.* **1997**, *36*, 1247.
[20] G. M. Sheldrick, *Acta Crystallogr. Sect. A Found. Crystallogr.* **2008**, *64*, 112.
[21] G. M. Sheldrick, *Acta Crystallogr. Sect. C Struct. Chem.* **2015**, *71*, 3.
[22] Bruker AXS Inc., *APEX II* **2013**.
[23] *Mercury, Version 3.3*, CCDC, Available Online Via Ccdc. Cam. Ac. Uk/Products/Mercury, n.d.
[24] L. J. Farrugia, *J. Appl. Cryst.* **2012**, *45*, 849.
[25] C. Yamazaki, *Can. J. Chem.* **1975**, *53*, 610.
[26] J. Gradinaru, A. Forni, Y. Simonov, M. Popovici, S. Zecchin, M. Gdaniec, D. E. Fenton, *Inorg. Chim. Acta* **2004**, *357*, 2728.
[27] B. Kaya, B. Ülküseven, O. Şahin, Z. S. Şahin, *J. Mol. Struct.* **2019**, *1191*, 337.
[28] Ö. Kurt, A. Koca, A. Gül, M. Burkut Koçak, *Synth. Met.* **2015**, *206*, 72.
[29] M. J. Frisch, G. W. Trucks, H. B. Schlegel, G. E. Scuseria, M. A. Robb, J. R. Cheeseman, G. Scalmani, V. Barone, B. Mennucci, G. A. Petersson, Wallingford CT **2009**, *93*.
[30] A. D. Becke, *J. Chem. Phys.* **1993**, *98*, 5648.
[31] C. Lee, W. Yang, R. G. Parr, *Phys. Rev. B* **1988**, *37*, 785.
[32] J. B. Foresman, A. Frisch, Exploring Chemistry With Electronic Structure Methods: A Guide To Using Gaussian, **1996**.
[33] P. J. Hay, W. R. Wadt, *J. Chem. Phys.* **1985**, *82*, 270.
[34] P. J. Hay, W. R. Wadt, *J. Chem. Phys.* **1985**, *82*, 299.
[35] W. R. Wadt, P. J. Hay, *J. Chem. Phys.* **1985**, *82*, 284.
[36] R. Apak, K. Güçlü, M. Özyürek, S. E. Karademir, *J. Agric. Food Chem.* **2004**, *52*, 7970.
[37] C. Sánchez-Moreno, J. A. Larrauri, F. Saura-Calixto, *J. Sci. Food Agric.* **1998**, *76*, 270.
[38] V. Suni, M. R. Prathapachandra Kurup, M. Nethaji, *Polyhedron* **2007**, *26*, 5203.
[39] A. Banerjee, A. Frontera, S. Chattopadhyay, *Dalton Trans.* **2019**, *48*, 11433.
[40] A. D. Khalaji, M. Amirnasr, S. Triki, *Inorg. Chim. Acta* **2009**, *362*, 587.
[41] A. D. Khalaji, H. Hadadzadeh, K. Fejfarova, M. Dusek, *Polyhedron* **2010**, *29*, 807.
[42] B. Kaya, K. Kaya, A. Koca, B. Ülküseven, *Polyhedron* **2019**, *173*, 114130.
[43] B. Ilhan-Ceylan, E. Tuzun, Y. Kurt, M. Acikgoz, S. Kahraman, G. Atun, B. Ulkuseven, *J. Sulfur Chem.* **2015**, *36*, 434.
[44] B. Kaya, A. Koca, B. Ülküseven, *J. Coord. Chem.* **2015**, *68*, 586.
[45] Y. Kurt, A. Koca, M. Akkurt, B. Ülküseven, *Inorg. Chim. Acta* **2012**, *388*, 148.
[46] M. Şahin, A. Koca, N. Özdemir, M. Diner, O. Büyükgüngör, T. Bal-Demirci, B. Ülküseven, *Dalton Trans.* **2010**, *39*, 10228.
[47] H. Bahron, S. S. Khaidir, A. M. Tajuddin, K. Ramasamy, B. M. Yamin, *Polyhedron* **2019**, *161*, 84.
[48] R. G. Parr, R. G. Pearson, *J. Am. Chem. Soc.* **1983**, *105*, 7512.
[49] R. G. Parr, L. V. Szentpály, S. Liu, *J. Am. Chem. Soc.* **1999**, *121*, 1922.
[50] M. Tümer, *Synth. React. Inorganic, Met. Nano-Metal Chem.* **2011**, *41*, 211.
[51] C. M. Sharaby, *Spectrochim. Acta - Part a Mol. Biomol. Spectrosc.* **2007**, *66*, 1271.
[52] Ö. Özdemir, *J. Photochem. Photobiol. A Chem.* **2020**, *392*, 112356.
[53] V. Butkovic, L. Klasinc, W. Bors, *J. Agric. Food Chem.* **2004**, *52*, 2816.
[54] D. Villaño, M. S. Fernández-Pachón, M. L. Moyá, A. M. Troncoso, M. C. García-Parrilla, *Talanta* **2007**, *71*, 230.
[55] J. Xie, K. M. Schaich, *J. Agric. Food Chem.* **2014**, *62*, 4251.
[56] D. T. Nguyen, T. H. Le, T. T. T. Bui, *Eur. J. Med. Chem.* **2013**, *60*, 199.

[57] J. Sochor, J. Dobes, O. Krystofova, B. Ruttkay-Nedecky, P. Babula, M. Pohanka, T. Jurikova, O. Zitka, V. Adam, B. Klejdus, R. Kizek, *Int. J. Electrochem. Sci.* **2013**, *8*, 8464.
[58] S. Rey, E. Gómez, H. Muñoz-Cimadevilla, D. Hevia, *In Vivo (Brooklyn)* **2018**, *54*, 339.

Note. All potentials are given versus Ag/AgCl.

SUPPORTING INFORMATION

Additional supporting information may be found online in the Supporting Information section at the end of this article.

How to cite this article: Kaya B, Akyüz D, Karakurt T, Şahin O, Koca A, Ülküseven B. Cobalt (II)/(III) complexes bearing a tetradentate thiosemicarbazone: Synthesis, experimental and theoretical characterization, and electrochemical and antioxidant properties. *Appl Organomet Chem*. 2020;34:e5930. https://doi.org/10.1002/aoc.5930